

Validation of Microwave Sea Surface Temperature Measurements for Climate Purposes

DETLEF STAMMER

Physical Oceanography Research Division, Scripps Institution of Oceanography, La Jolla, California

FRANK WENTZ AND CHELLE GENTEMANN

Remote Sensing Systems, Santa Rosa, California

(Manuscript received 10 January 2002, in final form 22 July 2002)

ABSTRACT

A comparison is provided between recent SST observations obtained from the TRMM Microwave Imager (TMI) with the commonly used Reynolds and Smith SST analysis and in situ data that highlights the significant value added by the microwave SST observations above what can be obtained from infrared technology. The largest benefit of the microwave technology clearly comes from the unprecedented near all-weather sampling of ocean phenomena that yields measurements of ocean SST without the heavy smoothing in space and time that is traditionally being applied to close data gaps resulting from clouds. This comparison of the TMI fields with the Reynolds and Smith analysis results in a mean offset of 0.18°C and a standard deviation (STD) difference of 0.54°C over the latitude range $\pm 36^\circ$. Regionally STD differences are found between both SST fields that reach 1°C or more, a number that is significantly larger than the error specification of either dataset alone. STD differences are obtained between Reynolds and Smith and in situ data of 0.55°C as compared to only 0.45°C from the TMI fields. Moreover, those uncertainties are time dependent and spatially varying, revealing a clear seasonal cycle with amplitudes varying by 0.35°C in the Reynolds and Smith SST fields around 25° latitude on the annual cycle in both hemispheres. Both TMI and the Reynolds and Smith analyses show temporal trends relative to in situ observations that differ in sign and amplitude.

1. Introduction

To date, many studies of sea surface temperature (SST) are based on fields such as the Reynolds and Smith (1994, hereafter RS94) weekly SST analysis. These gridded SST fields provide one of the longest datasets in the history of ocean remote sensing, which has proven to be of significant value for climate research. They are produced from a combination of Advanced Very High Resolution Radiometer (AVHRR) measurements and in situ observations. But since the major component of the RS94 SST fields are the AVHRR measurements, these fields are plagued by the disadvantages associated with infrared observations, especially the limited sampling due to cloud cover. Resulting data gaps are usually filled through a space-time objective analysis that provides heavily smoothed fields of SST. At the same time, the satellite SST measurements are also converted from skin to bulk temperatures and corrected for the effect of aerosols on the SST retrieval.

Recently, the technology of microwave imaging has provided an alternative source of SST measurements. This new technology is currently implemented on the Tropical Rainfall Measuring Mission (TRMM) satellite (Wentz et al. 2000) that was launched late in 1997 into an orbit with an inclination of 35° and provides a nearly complete SST sampling every two days roughly between $\pm 38^\circ$ latitude. Measurements are taken over the 10.7–85.6-GHz band (Kummerow et al. 1998). Despite its disadvantage of having a significantly larger footprint of around 47 km (diameter), the tremendous advance of the microwave technology is that it provides all-weather measurements and thus allows dramatically improved spatial and temporal sampling over the entire ocean. As can be seen from Fig. 1, the TRMM Microwave Imager (TMI) provides almost 100% data coverage with only minor dropouts due to intense rain events (mostly tropical). In contrast the infrared multi-channel SST (MCSST) fields have a maximum retrieval rate of only 80% and then only in subtropical regions. More common for this sensor, however, is a data coverage of less than 40%, especially in midlatitudes and over the intertropical convergence zone (ITCZ), where, therefore, a significant fraction of the dynamically interesting ocean signal cannot be sampled by this technology. In climate-relevant subpolar regions the data return is usu-

Corresponding author address: Detlef Stammer, Physical Oceanography Research Division, Scripps Institution of Oceanography, 9500 Gilman Dr., La Jolla, CA 92093-0230.
E-mail: dstammer@ucsd.edu

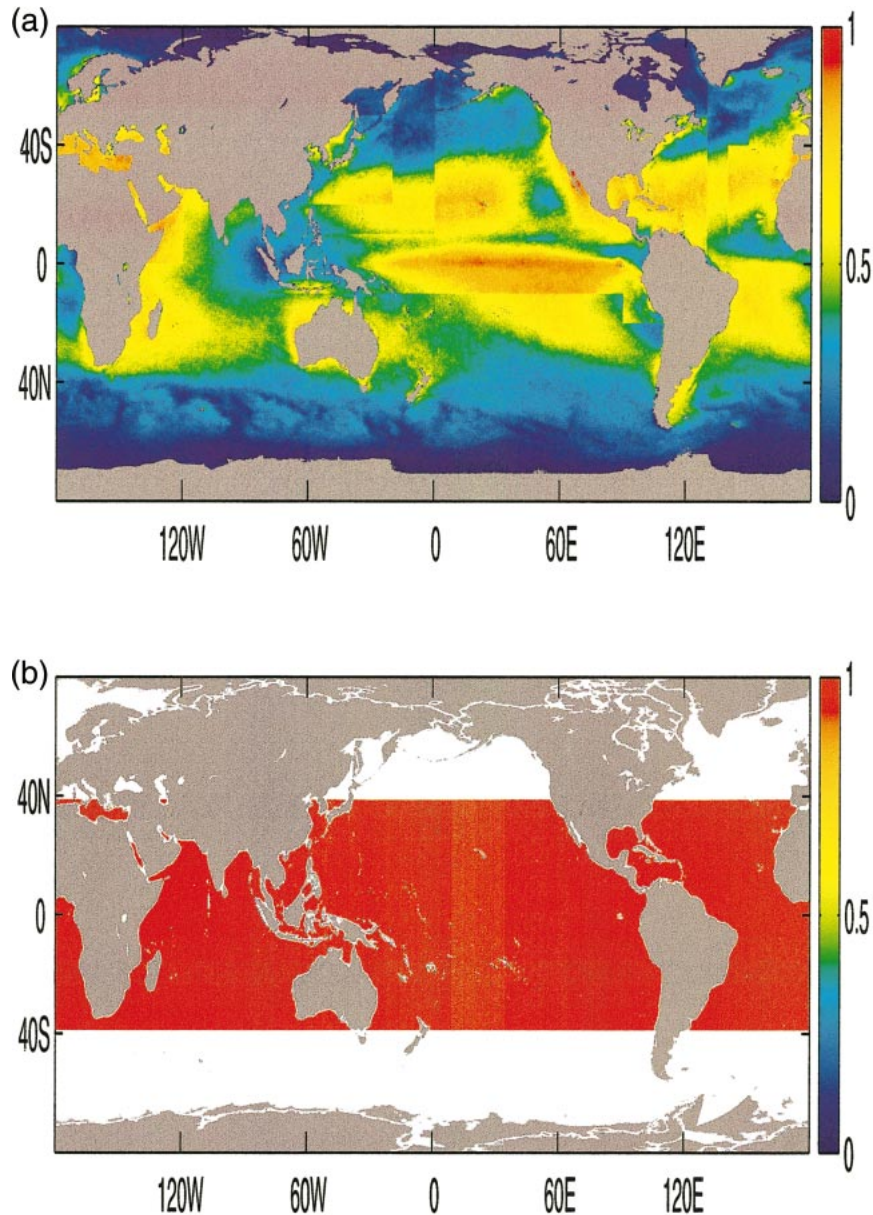


FIG. 1. Percentage data coverage of the (a) MCSST and (b) TMI for the 3-yr period 1998–2000. The TMI data coverage reflects the actual sampling of the TRMM satellite roughly between $\pm 38^\circ$ lat. We note that the block structures in (a) reflect the actual MCSST data distribution that is input for the Reynolds and Smith (1994) analysis, which reflects the NOAA SST data priorities for different regions. Low priority areas are processed only at a 50-km sampling rate, while high priority areas are processed with maximum resolution (5 km).

ally not more than 10%. Infrared sensors, therefore, pose a serious limitation for providing observations in those climate-relevant regions.

The purpose of this study is to document the high quality of the TMI SST fields for climate research purposes by comparing them with the RS94 SST fields and in situ observations. The basis of this study is the TMI data from the period January 1998–June 2001 as described by Wentz (1998). The microwave temperature

of the sea surface in the 10-GHz band depends primarily on SST and wind speed. The wind effect is eliminated from the measured brightness temperatures using information in both the horizontally and vertically polarized channels, thus providing a unique relation between the measured brightness temperatures and SST. Heavy rain events can contaminate TMI observations; however, those events can easily be identified and eliminated from further analysis. Additional contaminations occur when

islands or a coastline reach into the antenna footprint of the microwave instrument. See Wentz et al. (2000) and C. L. Gentemann et al. (2002, unpublished manuscript) for details on the TMI retrieval algorithm. Previously, Chelton et al. (2000) used TMI data to demonstrate unprecedented observational evidence of tropical instability waves on both sides of the equator. Similar to their approach, the TMI swath data were interpolated here every week onto a regular $1^\circ \times 1^\circ$ spatial grid using the three-dimensional Loess smoother described by Schlax and Chelton (1992) with smoothing parameters of $2^\circ \times 2^\circ$ in latitude and longitude and 14 days in time. Weekly RS94 analyses are available on the same space–time grid from the identical period.

In section 2 we will provide a general discussion of the differences between the RS94 and TMI fields. Section 3 provides a discussion of the differences between both SST datasets to in situ data that will be used to analyze trends in one or both of them and to shed light on an apparent seasonal cycle in the SST differences. Section 4 concludes with a summary and perspective.

2. TMI–Reynolds differences

We will begin by establishing a quantitative comparison between the TMI and RS94 SST fields. The seasonal cycle in SST accounts for most of the signal variance in SST data (95% for the RS94 data). Amplitudes of the annual harmonic range from less than 1°C in the tropical regions to almost 10°C in western boundary current regions (Fig. 2). Typical amplitudes of the annual harmonic are around 4°C in the open ocean away from the equator and increase toward all ocean boundaries. The annual harmonic phase shows that the maximum SST occurs around day 250 in the Northern Hemisphere tropical oceans, and slightly earlier in the mid-latitudes and western subtropical regions. The Southern Hemisphere SST variations are shifted in phase by about 180° according to the solar insolation cycle there. In the Indian Ocean north of the equator, the annual maximum SST occurs about three months earlier than in both the North Atlantic and North Pacific, but the phase is modulated by regional circulation structures there, such as the Great Whirl (see also below).

It is clear from the figure that variations in SST are relatively small and that accuracies of SST retrievals are quite demanding. Of specific interest for climate studies are SST variations outside the annual frequency band, especially on interannual and longer timescales. As an example we show in Fig. 3 the differences of annual mean TMI SST fields from year 2000 minus those from 1998. While in the tropical Pacific ENSO-related SST anomalies are quite prominent, the largest positive variations are visible in the subtropical North Pacific and North Atlantic where large-scale anomalies of 2°C and more are quite common. In contrast, the Southern Hemisphere shows predominantly colder temperatures in 2000 relative to 1998 by -1° to -2°C . To

indicate that those interannual changes are physical signals that can be related to changes in large-scale ocean dynamics or heat content, we show in Fig. 3b the similar difference as before, but now for TOPEX/Poseidon (T/P) altimetric sea surface height (SSH) measurements. There is clearly a complex relation between both remote sensing fields that does not allow a simple interpretation or inference of one from the other. Nevertheless, they both show anomalies along the same large-scale pattern, for example, those crossing the Pacific Ocean in a ridge-like pattern from the western tropical Pacific to mid-latitude positions at the eastern side of the basins. Likewise similar anomaly patterns are visible in the Indian Ocean. As will become clear below, many of those patterns that characterize the interannual SST and SSH variations will reappear in the difference fields between TMI and RS94 data—a fact that has implications for the interpretation of differences between the two SST datasets (see below).

To be more specific about observed SST variations, Figs. 4a–c show examples of TMI and RS94 SST time series from three different, but characteristic, locations in the Pacific Ocean. A local 3-yr time-mean value was removed from each time series previously. Overall, both fields track each other closely and their variations are dominated by the seasonal cycle shown as a red curve. Superimposed to the seasonal cycle are higher-frequency changes with amplitudes of 1° or less. We note also that the RS94 and TMI time series show distinct longer-period variations visible here as deviations from the long-term seasonal cycle. At the northern position (Fig. 4a) relatively colder (by more than 1°C) SST observations occurred during the last ENSO event, while close to the equator (Fig. 4b) SST was warmer by several degrees during 1998, but mostly colder than the climatological seasonal cycle during the subsequent years. At the southernmost (Fig. 4c) location, we find again significant deviations from the climatological seasonal cycle, especially over the first year.

Our goal here is to compare the two SST datasets against each other and later both against in situ data. We show therefore in Figs. 4d–f differences between TMI minus RS94 SST observations from the same locations that reveal biases of up to 0.5°C in the Southern Hemisphere (i.e., the RS94 analysis is colder than TMI fields). A full map of the time-mean difference is provided in Fig. 5a and reveals a complex geographical bias pattern. While the Southern Hemisphere and the North Atlantic show generally positive differences, the eastern Pacific is colder in the TMI fields, as is the Indian Ocean and the Kuroshio Extension. The mean difference between the TMI fields and the RS94 analysis is 0.18°C over the latitude range $\pm 38^\circ$.

In addition to the bias, many regions are also characterized by a pronounced trend between the two SST observations that leads to regionally increased TMI SST values by up to 1°C as compared to RS94, especially over the South Pacific, but also over other regions of

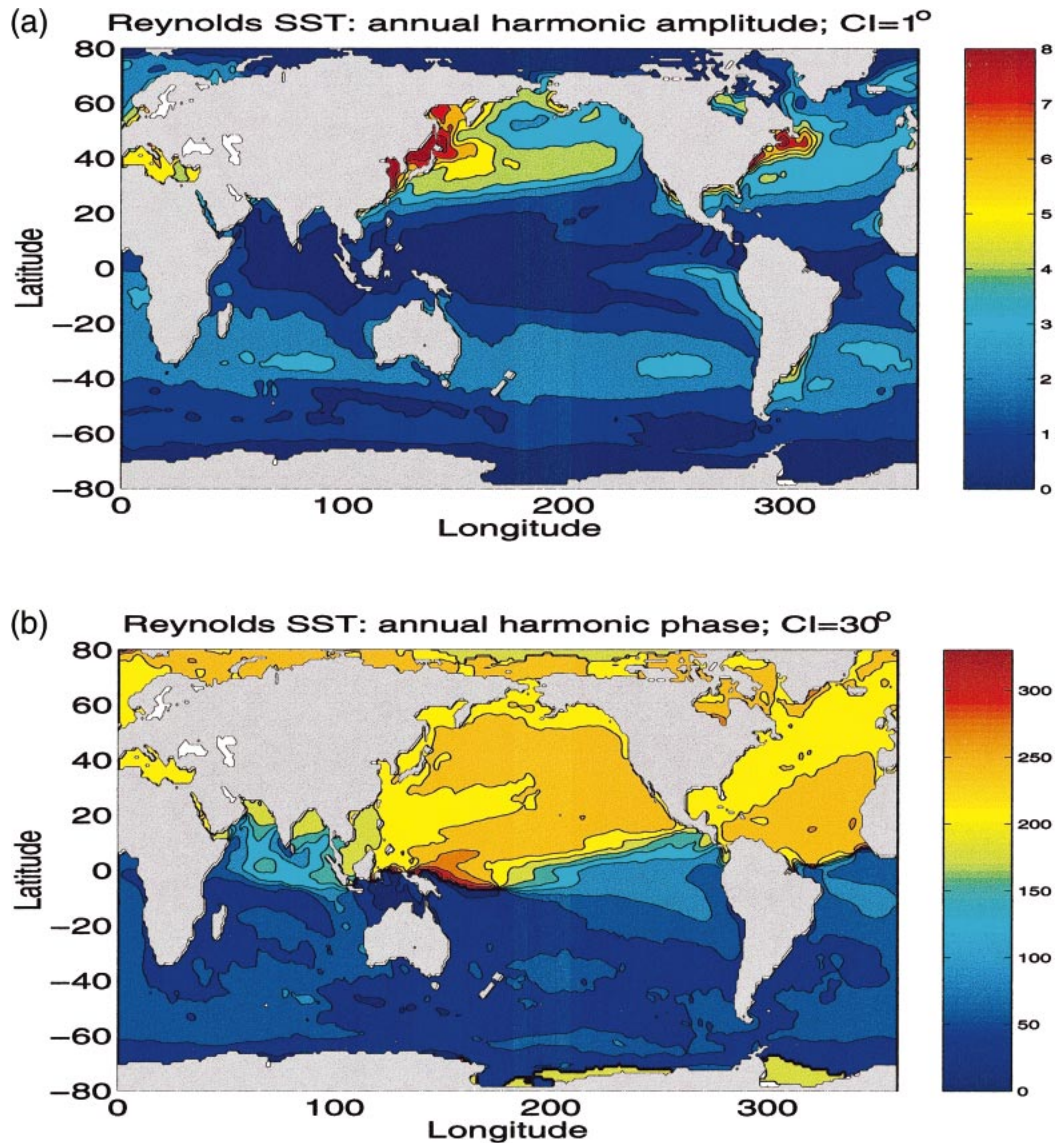


FIG. 2. (a) Annual harmonic amplitude of the Reynolds and Smith (1994) SST estimated for the 7-yr period 1993–2000. Contour interval is 1°C. (b) Annual harmonic phase from the same period in degrees relative to Jan.

the Southern Hemisphere (Fig. 5b). Trends were estimated here by a local least squares fit of a straight line to the 3-yr-long difference time series. In contrast to the Southern Hemisphere, many TMI SST values seem to decrease in the Northern Hemisphere relative to the Reynolds analysis, for example, near the North Brazil Current, along the California coast, and at the western side of the Pacific. Likewise most of the central Indian Ocean appears to become colder in TMI observations. The mean temporal trend between the TMI fields and the RS94 analysis is 0.26°C over the analyzed 3-yr period.

A comparison between Figs. 5a and 5b reveals that regions of positive and negative biases mostly coincide with those of positive and negative trends in the SST

differences, suggesting that the bias does not simply represent a systematic difference, but to some extent it also reflects the effect of the temporal trend in one or both of the datasets. Equally important, a comparison of Fig. 5b with Fig. 3 reveals that the drift of the SST difference fields is quite similar to the pattern of large-scale interannual changes in SST and SSH: note especially the positive values in all of those fields in the western tropical Pacific and from there reaching northeast and southeastward across the basins. Although interannual changes are larger, the drifts are of comparable amplitude. An understanding of the bias and trend pattern in the SST fields is therefore of considerable concern for quantitative SST-related climate studies.

In principle, temporal trends between both SST fields

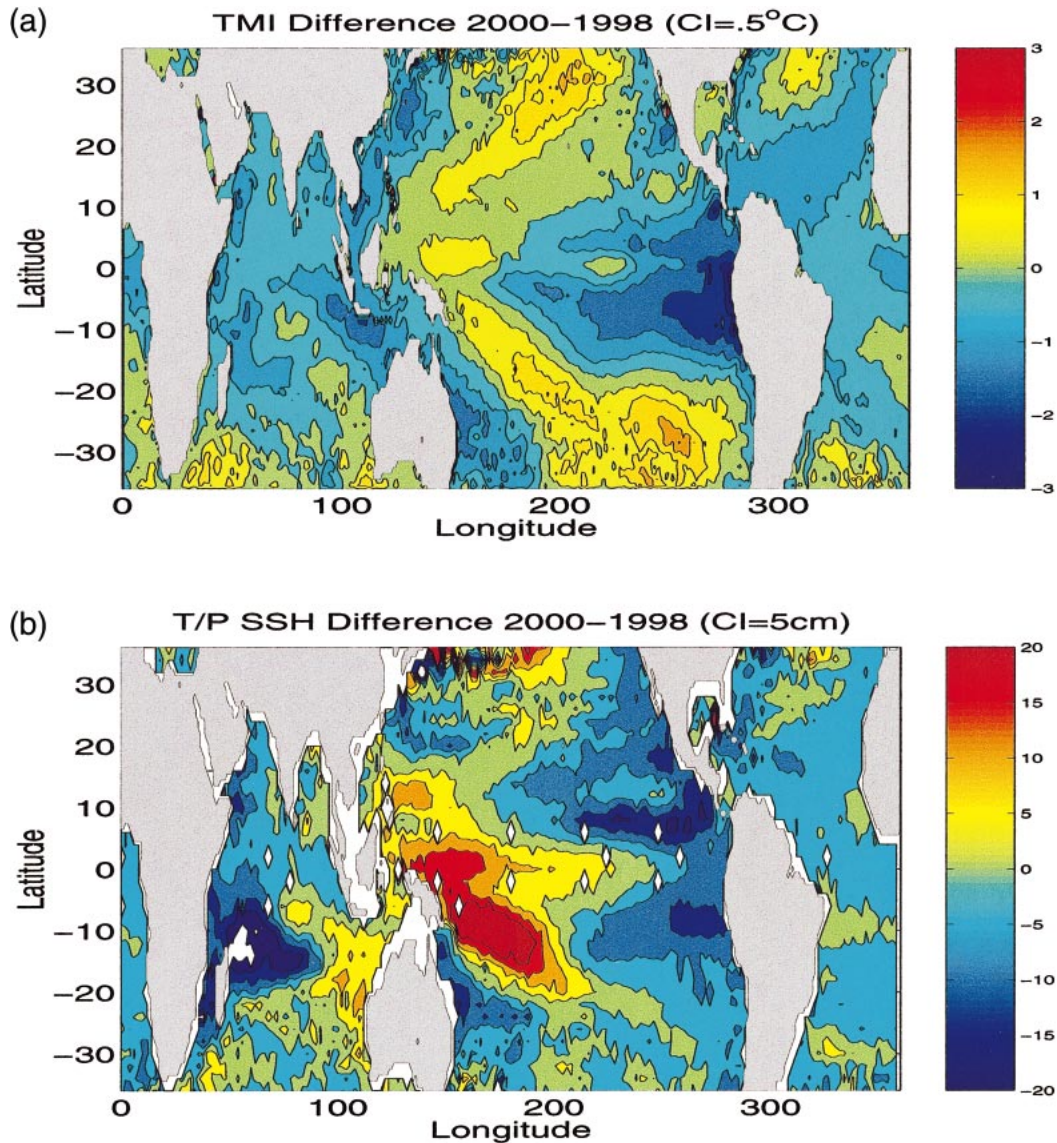


FIG. 3. Differences in (a) SST and (b) SSH between the annual mean of year 2000 minus that from 1998. Contour intervals are 0.5°C and 5 m, respectively.

could also result in a distinct pattern of the standard deviation (STD) of the difference between both fields. However, this is not the case (Fig. 6). Instead, the resulting STD difference pattern clearly points toward oceanic variability structures. We note that the STD differences are strikingly small (about 0.2°C) over the subtropical gyres, implying that an uncorrelated white noise floor in the difference fields has to be smaller than that number. However, the STD differences reach values of 1°C or even more in other regions, especially along 30°N over both the Pacific and Atlantic. The mean STD difference between the TMI fields and the RS94 analysis is 0.54°C .

To demonstrate that a large fraction of the STD differences arises from enhanced amplitude SST variability

in the TMI fields, Fig. 6b shows the standard deviation of the TMI fields while Fig. 6c shows the STD (RS94) field. From both datasets the climatological seasonal cycle was removed previously; that is, the two latter fields represent only the nonseasonal variability. Although both panels show similar spatial patterns that in turn agree with those present in Fig. 6a, the TMI field exhibits substantially more energy, especially in mid latitudes. Note also the clear presence of a pattern in the TMI SST variability field associated with the Tehuanapec and Papagayo wind jets and their effect on SST off the southern coast of Central America, the enhanced variability off the coast of California, the enhanced variability off North Africa, in the Indian Ocean, and generally along all coasts and islands. Clearly the

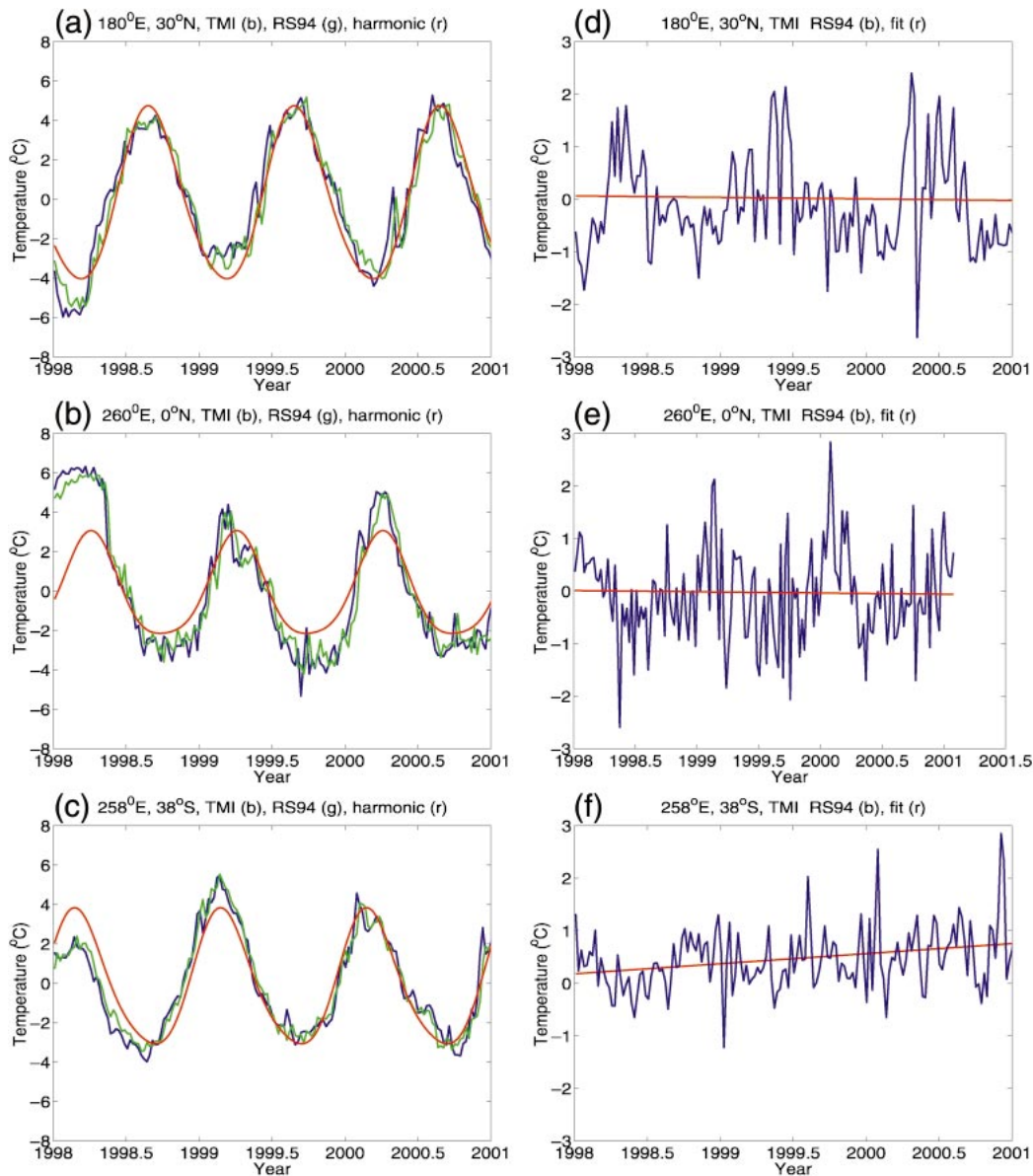


FIG. 4. (a)–(c) Time series of TMI (blue) and RS94 SST fields (green) at several characteristic locations: (a) 30°N, 180°; (b) 0°, 260°E; (c) 38°S, 250°E. Also shown in red is the annual harmonic evaluated at those locations from the RS94 fields over the 7-yr period 1993–2000. (d)–(f) Differences between TMI and RS94 fields at the locations (a)–(c) and linear trend fitted over the 3-yr period (green).

RS94 dataset underestimates all those processes (Fig. 6c) that often occur on relatively small spatial and/or temporal scales. Along the same lines, the SST variability in the vicinity of the Kuroshio Current and the Gulf Stream Extension is largely absent in the RS94 fields (cf. also D. Stammer et al. 2002, unpublished manuscript). Accordingly, the TMI data show an enhanced SST variance in those regions by up to a factor of 4 (a factor of 2 in STD) as compared to the RS94 analysis.

To provide a better description of spatial variations in the differences, Fig. 7 displays typical difference

fields between TMI and Reynolds observations from the eastern tropical Pacific and the Indian Ocean along with the individual TMI and RS94 fields. Differences of $\pm 2^{\circ}\text{C}$ and more are quite common over large fractions of the figure panels. Obviously those differences are far from being white noise but, instead, display eddy-or wavelike structures that are not present in the RS94 fields.

In the Arabian Sea every year a distinct eddylike feature appears in the Somali basin in late summer that is usually referred to as the “Great Whirl.” Schott and McCreary (2001) give a detailed review of the

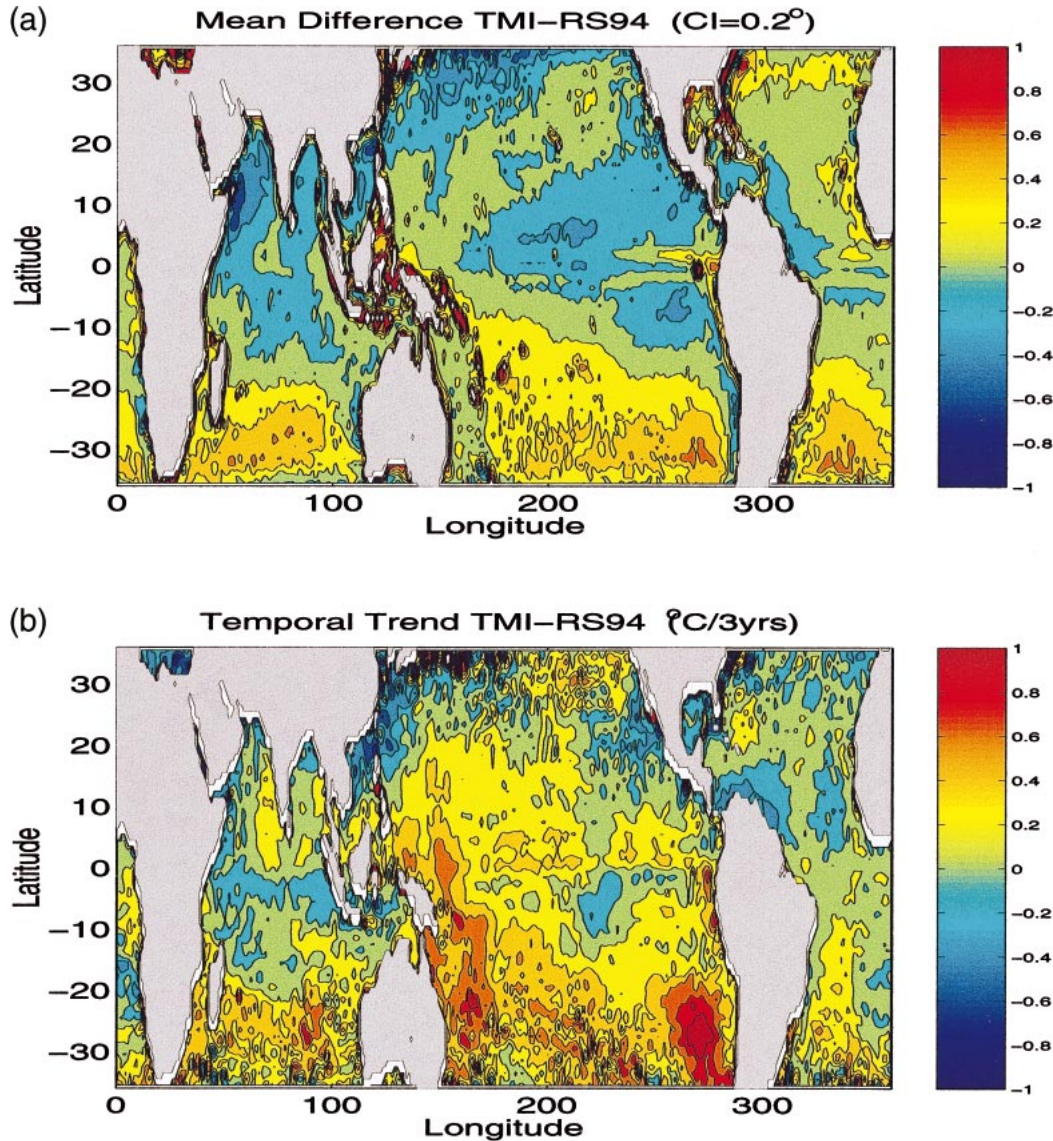


FIG. 5. (a) Mean and (b) linear trend of the difference between TMI and RS94 SST datasets from the period 1998–2000. Zonal averages of both fields are displayed in Fig. 9. Contour intervals are 0.2°C . Global mean difference is 0.18°C .

monsoon circulation of the Indian Ocean and its variation on various time- and space scales. An anomalous dipole mode in the Indian Ocean SST field with warmer than normal water in the western Indian Ocean and cooler than normal waters in the eastern basin are believed to be responsible for heavy rainfall over east Africa and a weaker monsoon over the Indian continent (Webster et al. 1999; Murtugudde et al. 2000; Saji et al. 1999). Detailed information about SST variations are therefore critical for many countries around the Indian Ocean. As can be seen from Fig. 7a the TMI data from late September of 1998 show a filament of cold water reaching from the coast of Somali into the Somali basin as is typical for the

development of the Great Whirl. At the same time the northern Arabian Sea is characterized by a ridge of warm water reaching zonally across the basin. Both features are fairly underrepresented in the respective RS94 field (Fig. 7c) and exist there only on large spatial scales. Accordingly, the difference field is dominated by those and other similar small-scale features that represent real physical signals in the TMI data (Fig. 7e).

A second example is provided from the eastern tropical Pacific from 15 September 1999. In this region cold water appears first near the continental coast and then propagates westward along the equator. Those phenomena are associated with instability events of the regional

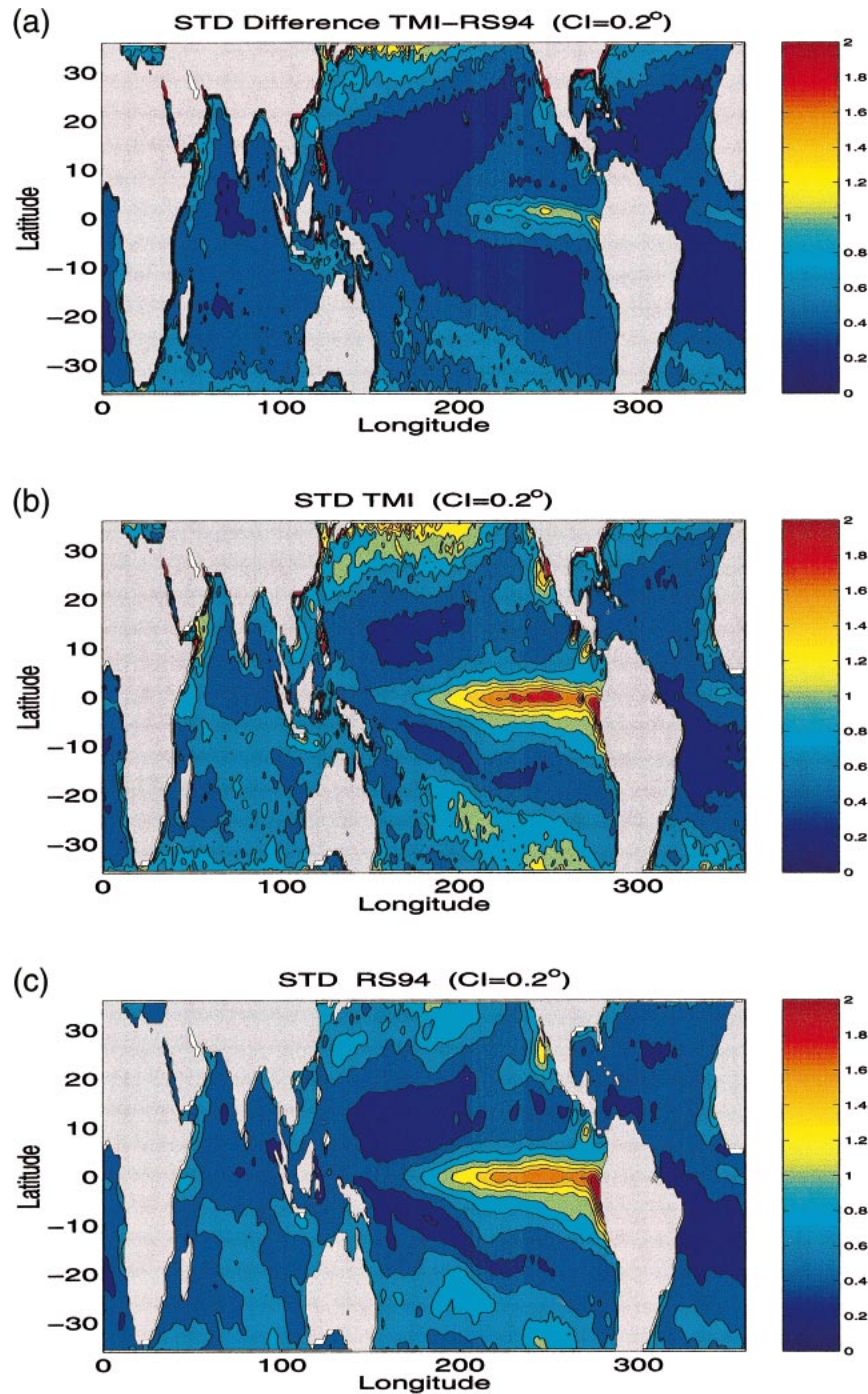


FIG. 6. (a) STD of the difference between TMI and Reynolds data over 3-yr period. Global STD difference is 0.54°C . (b), (c) STD of TMI nonseasonal SST anomaly fields from the period 1998–Jun 2000 and STD of the nonseasonal RS94 SST anomaly fields. See text for details. Contour interval is 0.2°C .

circulation that are usually referred to as tropical instability waves (TIW). See Chelton et al. (2000) for a detailed description of those TIW phenomena as seen by TMI. Both the cold tongue and the smaller-scale anomalies associated with the instability waves are

clearly visible in the temperature anomalies from 15 September 1999 (Fig. 7b). Note again the cold small-scale SST anomalies in the TMI field close to the Central American continent as they result from the Tehuanapec and Papagayo wind jets and related mixing and up-

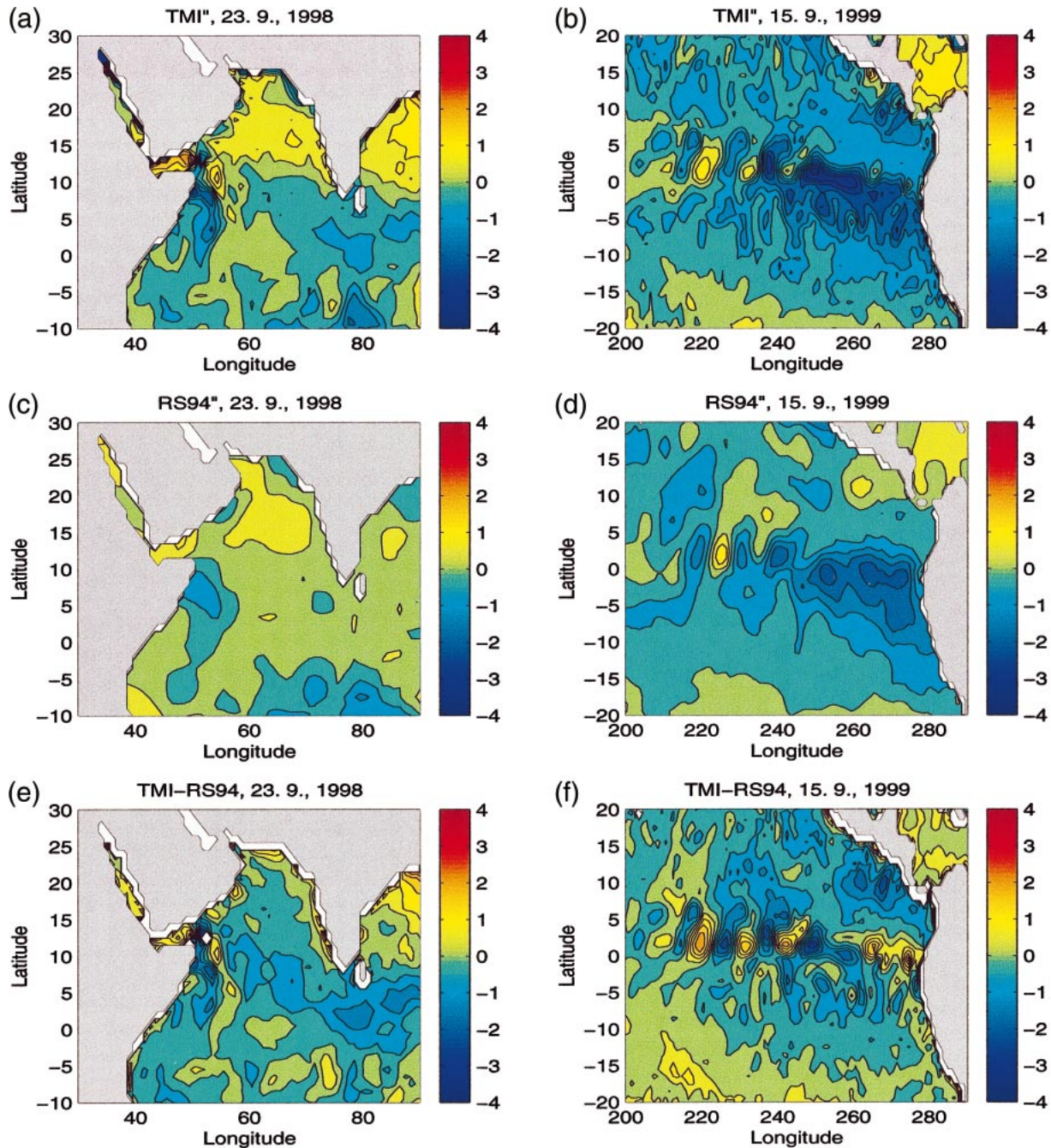


FIG. 7. Nonseasonal TMI SST anomalies shown (a) from the week centered around 23 Sep 1998 in the Indian Ocean, and (b) centered around 15 Sep 1999 in the tropical Pacific. (c), (d) Similar fields, but from the RS94 analysis. (e), (f) Difference fields TMI - RS94. Contour intervals are 0.5°C.

welling. Again all those smaller-scale structures associated with ocean dynamics are severely underrepresented in the RS94 field.

3. Comparison with in situ data

Most previous figures showed aspects of the complicated nature of the differences between the two SST

datasets that for quantitative climate studies can pose problems if we are not able to identify their cause. However, without any extra information, their origin cannot be easily understood. To identify the SST dataset that causes those problems, we will use in the following the extra information available from four in situ datasets of near-surface temperature observations obtained from surface drifters, the Profiling Autonomous Lagrangian

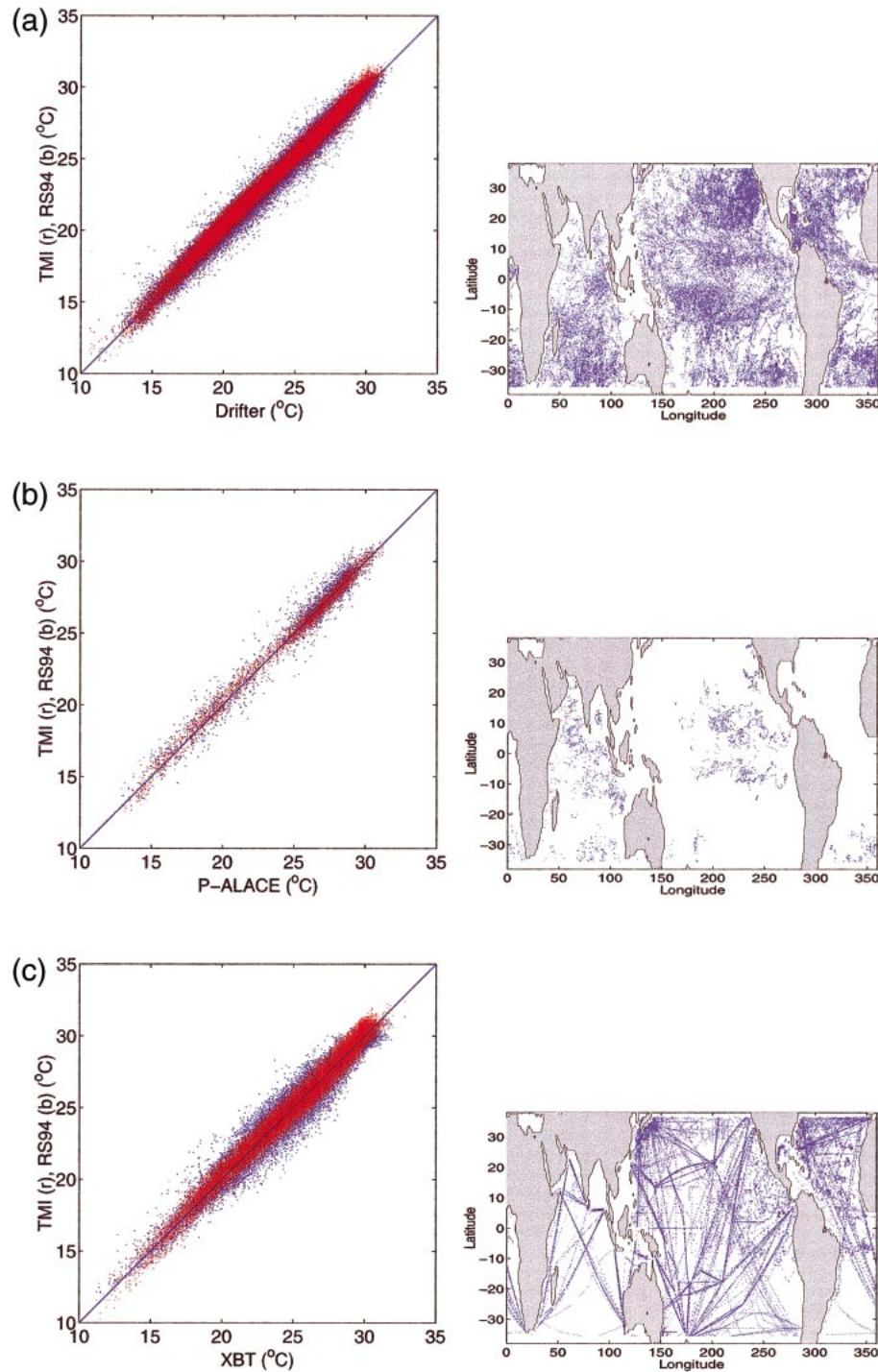


FIG. 8. Scatterplot of TMI (red) and RS94 (blue) fields against surface temperature observations obtained from (a) surface drifter, (b) PALACE floats, and (c) XBT and TAO measurements. The respective data distributions are shown in the insets on the right side.

Circulation Explorer (P-ALACE) floats, and the expendable bathythermograph (XBT) and Tropical Atmosphere Ocean (TAO) measurements (McPhaden et al. 1998). The geographical distribution of the in situ data is shown in the right panels of Fig. 8. Although

none of the measurements directly sample the skin SST, they all measure the near-surface region above 6-m depth, some close to the surface.

SST observations are obtained by the surface drifters through measurements at 0.1-m depth as explained in

TABLE 1. Mean difference between TMI (T) and RS94 (R) datasets and drifter (D) and XBT-TAO (X) observations, respectively.

Lat	T-D	R-D	T-R	T-X	R-X	T-R	$\overline{\delta T}$	$\overline{\delta R}$	$\overline{T - R}$
25°-35°N	0.11	-0.01	0.12	0.16	0.01	0.14	0.14	0.0	0.13
15°-25°N	0.13	0.05	0.09	0.03	0.00	0.03	0.08	0.03	0.06
5°-15°N	0.02	0.06	-0.04	-0.07	-0.03	-0.04	-0.03	0.02	-0.02
5°S-5°N	0.12	0.09	0.03	-0.02	0.02	-0.04	0.05	0.06	-0.01
15°-5°S	0.20	0.07	0.13	0.07	-0.00	0.07	0.14	0.04	0.10
25°-15°S	0.33	0.05	0.28	0.19	0.01	0.18	0.26	0.03	0.23
35°-25°S	0.39	0.01	0.38	0.28	-0.01	0.29	0.33	0.0	0.34

detail by Niiler (2001). Since the surface drifter and TAO data have been used as input for the weekly RS94 analysis (see also Reynolds et al. 2002), the comparison performed here between the RS94 fields and those measurements is to some extent only a consistency check.

In contrast to the drifter and TAO data, the XBT and PALACE float measurements were not used in the RS94 analysis. The XBT and TAO data were extracted from the National Centers for Environmental Prediction (NCEP) real-time temperature datasets and represent the top 5 m of the ocean. The P-ALACE measurements are obtained from the profiling floats on their way up toward the surface and the data used for the comparison are the last observation taken before the float reaches the surface (usually from 5–6-m depth; with higher vertical sampling rate, measurements could be obtained closer to the surface). The float data are those available simultaneously to TMI measurements and that show basically no near-surface vertical temperature gradient (R. Davis 2001, personal communication). See Davis et al. (2001) for details on the float system and data.

Global biases between the TMI SST fields and the in situ data are 0.18°, -0.04°, and 0.03°C for the drifter data, the P-ALACE and the XBT-TAO measurements, respectively. For the same in situ data, the RS94 analysis shows mean differences of 0.04°, -0.14°, and 0.00°C, respectively. Those statistics vary, depending upon which set of in situ observations and its spatial sampling were used for the computations. As compared to the above overall mean bias of 0.18°C, the TMI-RS94 differences yield 0.14°, -0.11°, and 0.02°C, respectively, on the drifter, P-ALACE, and XBT-TAO data distribution. For the TMI-RS94 STD differences we obtain 0.45°, 0.67°, and 0.51°C; the respective mean number is 0.56°C. Comparisons like those provided here between SST fields and sparse near-surface in situ data are intended to reveal robust systematic findings from all in situ fields together that could identify problems in one or both of the SST fields.

In Table 1 we show the mean differences between the SST fields with drifter and XBT-TAO data as a function of latitude, respectively. The biases between the RS94 fields and both the drifter and XBT-TAO data stay below 0.1°C, while biases between the TMI fields and the drifter data are as high as 0.4°, and about 0.3°C relative to XBT data, both evaluated between 35° and 20°S. To increase the significance of either comparison alone, we

averaged the biases resulting from drifter and XBT-TAO observations to obtain combined bias estimates, shown in the last three columns of the table. Those latter numbers are also displayed in Fig. 9a as a function of latitude, jointly with zonal averages from Fig. 5a. The figure indicates that the mean differences in the Southern Hemisphere and around the northern turning point seem to originate primarily from the TMI fields while the RS94 fields stay generally close to the observed mean values (recalling that XBT data are independent from the RS94 analysis). In lower latitudes, however, biases in both SST datasets are negligible (<0.1°C).

The left panels of Fig. 8 show scatterplots of RS94 and TMI SST data against near-surface temperature observations from surface drifter (Fig. 8a), P-ALACE floats (Fig. 8b), and from XBT and TAO measurements (Fig. 8c). All basically agree in the sense that both SST datasets follow the in situ measurements but are scattered around the ideal line of 45°. A visual inspection of the figure indicates already that the scatter obtained from the TMI field is smaller than that obtained from RS94 fields. The STD differences between TMI and drifter data, P-ALACE, XBT-TAO data are 0.46°, 0.43°, and 0.46°C, respectively. Similar STD differences but based on RS94 result in 0.54°, 0.70°, and 0.56°C.

The above numbers represent “global” statistics; that is, they are based on all in situ data. In Table 2 we show similar STD differences between both SST fields and the drifter and XBT-TAO observations, respectively, but now as a function of latitude. The STD differences are also illustrated in Fig. 9b (shown as difference variances) based on XBT-TAO data. Again the TMI STD differences relative to both in situ datasets are smaller than those based on RS94 fields, throughout. In summary, it can be concluded from the SST-in situ data comparisons that the bias between both SST datasets mostly originates from TMI, while the STD of the difference is largely due to the lack of small-scale transients in smoothed RS94 fields.

In Table 3 we summarize the drift of both SST fields relative to drifter and XBT-TAO data as a function of latitude. As before, we average the drifts into one joint estimate that is displayed in Fig. 9c together with zonal averages of the field given in Fig. 4b. A robust result is that both SST datasets are drifting but in some regions with opposite sign. The TMI fields seem to drift roughly by 0.26° over the three years almost independent of

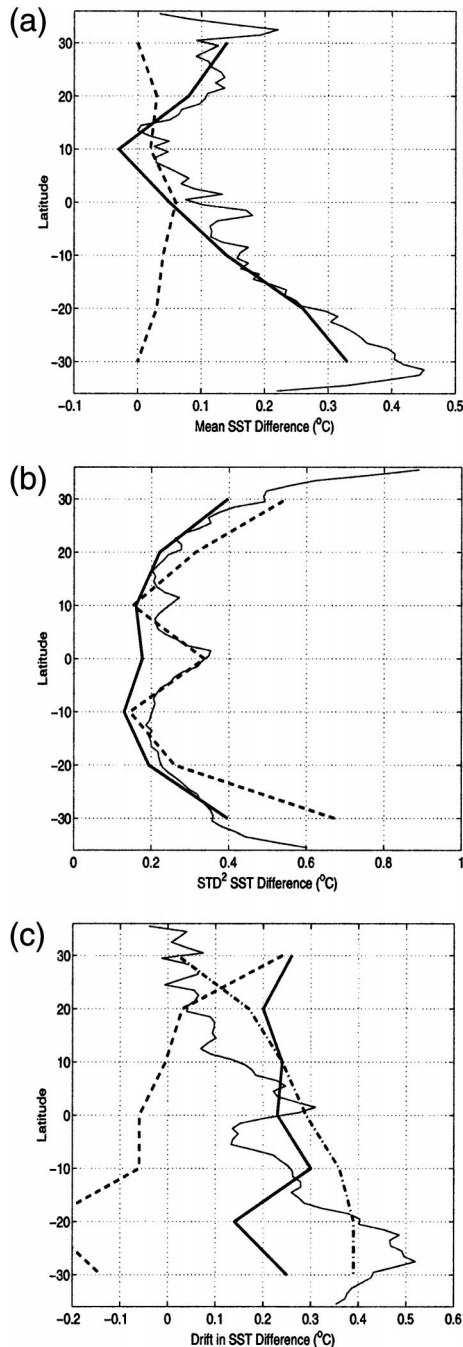


FIG. 9. (a) Zonally averaged biases between TMI and in situ (drifter and XBT observations) evaluated over 10° lat bands are shown by the bold solid line. Respective RS94-in situ data differences are shown as the dashed line. The thin solid line shows the zonal averages of the TMI-RS94 mean difference displayed in Fig. 5. Cf. to Table 1. (b): STD (TMI - in situ)² (bold solid), STD (RS94 - in situ)² (dashed). Also shown in STD (TMI - RS94)² (thin line) obtained as zonal average from Fig. 6a. Cf. to Table 2. (c): Drift between TMI and in situ (bold solid) and between RS94 and in situ data (dashed line), both estimated for the 3-yr period 1998–2000. The difference between the previous two lines (dashed-dotted line) represents the drift between both SST fields estimated on the in situ data position. It agrees basically with the thin line showing the zonal average from the TMI-RS94 drift displayed in Fig. 5b. See also Table 3.

TABLE 2. STD difference between TMI (T) and RS94 (R) datasets and drifter (D) and XBT-TAO (X) observations, respectively.

Lat	T-D	R-D	T-R	T-X	R-X	T-R
25°–35°N	0.47	0.64	0.54	0.63	0.82	0.71
15°–25°N	0.44	0.49	0.38	0.44	0.51	0.45
5°–15°N	0.40	0.42	0.35	0.36	0.38	0.39
5°S–5°N	0.40	0.48	0.42	0.42	0.58	0.49
15°–5°S	0.34	0.36	0.33	0.40	0.39	0.44
25°–15°S	0.42	0.50	0.39	0.47	0.56	0.51
35°–25°S	0.54	0.67	0.47	0.63	0.74	0.56

latitude. This relatively small drift over three years may be due to a slow deterioration in the TMI graphite antenna due to atomic oxygen in the ionosphere (Wentz et al. 2001). We note that C. L. Gentemann et al. (2002, unpublished manuscript) report a slightly smaller drift of 0.1°C over three years found from a comparison of TMI data with only the TAO data. In contrast, the RS94 fields drift by about the same amount but with opposite sign around 35°S , but $+0.2^\circ$ (3 yr^{-1}) around 35°N . Together both lead to the large drift of about 0.4°C found in the Southern Hemisphere relative to each other over the 3-yr analysis period. We note that the latitudinal dependence of the relative drift shown in Fig. 5b seems to arise entirely through the geographically varying drift in the RS94 fields.

Plotted in Figs. 10a,c are time series of the differences between drifter and RS94, and drifter and TMI for the latitude band 25° – 35°N for the years 1998–99. Figures 10b,d show the same but for XBT data. Amplitudes and phases of an annual harmonic fitted to the differences between SST data and drifter and SST and XBT observations are summarized in Table 4 separately for both RS94 and TMI data as a function of latitude. Note that both in situ datasets point consistently toward a clear seasonally varying error in the RS94 analysis with amplitudes ranging from about 0.3°C or more in midlatitudes and phases that change from a maximum around May over the Southern Hemisphere (late southern fall) to around November in the Northern Hemisphere (late boreal fall). We note that the temporal trend and the seasonal bias in the RS94 data are found relative to drifter and XBT data, although drifter data were being used in the RS94 analysis. A puzzling fact is also that the RS94 analysis is obviously biased low during local summer months and high in winter. This is counterintuitive since the summer months should show more stratification and thus higher SST relative to subsurface in situ data. An explanation for the seasonal cycle in the RS94 error is not at hand; however, it was also found by Reynolds et al. (2002) and is being discussed extensively by those authors.

A seasonal cycle in the respective TMI differences is significantly smaller (mostly smaller than 0.05°C). Present uncertainties in the TMI calibration relative to the surface roughness are about 0.1°C and thus as large as the amplitude of the seasonal cycle in the differences

TABLE 3. Drifts in TMI (T) and RS94 (R) fields relative to drifter (D) and XBT-TAO (X) datasets. The last three columns show the average of the respective previous differences.

Lat	T-D	R-D	T-R	T-X	R-X	T-R	$\overline{\delta T}$	$\overline{\delta R}$	$\overline{\delta T - R}$
25°-35°N	0.33	0.13	0.20	0.18	0.34	-0.16	0.26	0.24	0.02
15°-25°N	0.22	-0.05	0.28	0.18	0.11	0.06	0.20	0.03	0.17
5°-15°N	0.09	-0.06	0.15	0.39	0.05	0.33	0.24	-0.01	0.24
5°S-5°N	0.21	0.01	0.20	0.26	-0.13	0.39	0.23	-0.06	0.29
15°-5°S	0.20	-0.04	0.24	0.39	-0.08	0.48	0.30	-0.06	0.36
25°-15°S	-0.01	-0.19	0.18	0.28	-0.33	0.61	0.14	-0.26	0.39
35°-25°S	0.34	-0.04	0.38	0.15	-0.24	0.40	0.25	-0.14	0.39

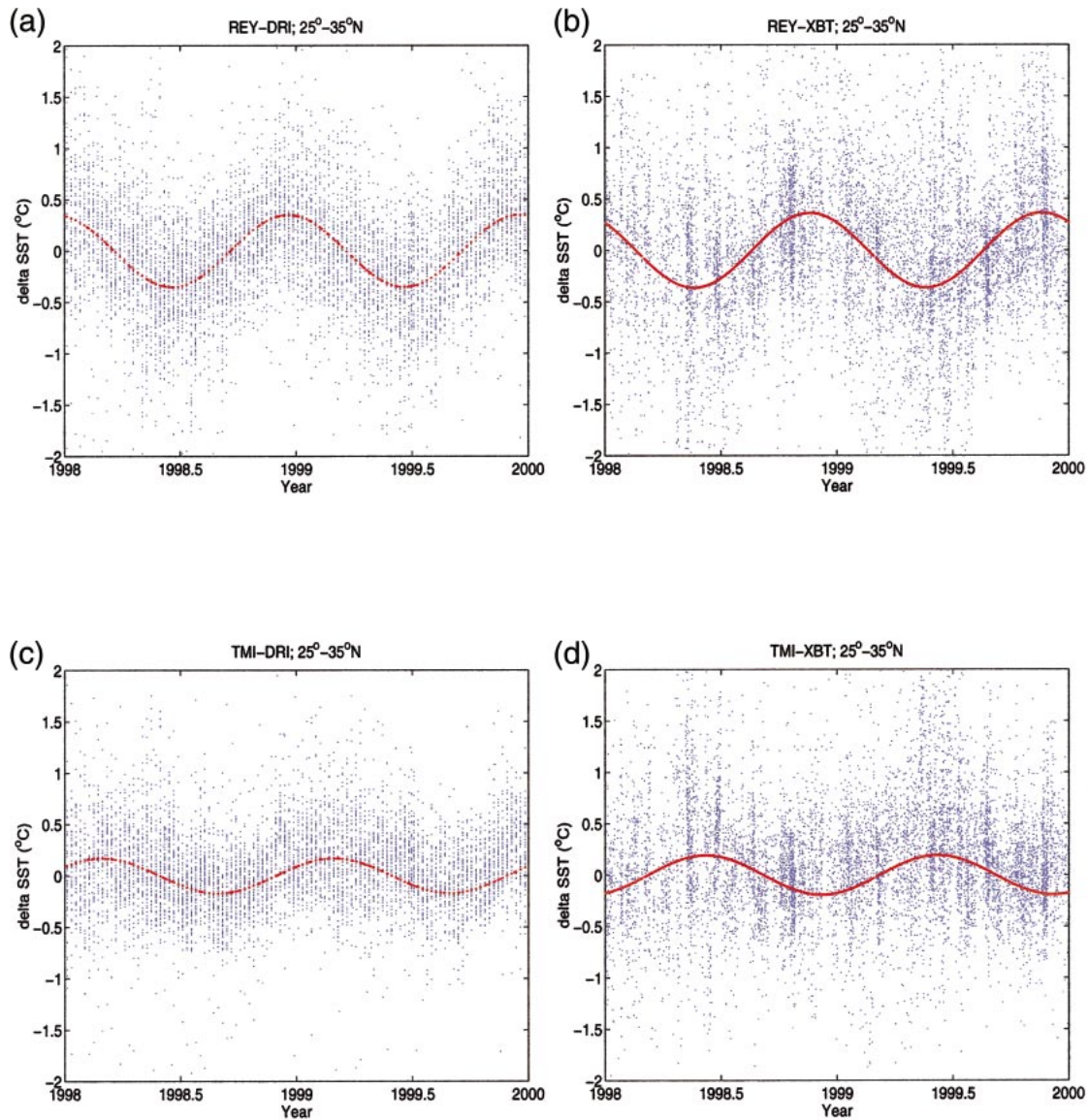


FIG. 10. Differences between RS94 and (a) surface drifter and (b) XBT temperature measurements displayed as a function of time from the latitude range 25°-35°N. (c), (d) The same differences but based on TMI data. The respective red curves in all panels show the annual harmonic fitted to all data in that latitude range. Amplitudes and phases of annual harmonics are summarized in Table 4 as a function of latitude.

TABLE 4. Annual harmonic in differences evaluated over the Pacific Ocean between 100° and 280°E longitudes.

Lat	T-D		R-D		T-X		R-X	
	Amplitude	Phase	Amplitude	Phase	Amplitude	Phase	Amplitude	Phase
25°–35°N	0.14	1.91	0.35	11.72	0.20	4.80	0.34	10.76
15°–25°N	0.11	1.95	0.24	11.72	0.11	4.16	0.14	11.54
5°–15°N	0.08	7.60	0.10	10.94	0.07	6.86	0.04	10.35
5°S–5°N	0.03	3.17	0.06	6.80	0.02	3.44	0.06	7.09
15°–5°S	0.01	4.23	0.11	5.52	0.07	11.43	0.07	5.95
25°–15°S	0.12	7.71	0.21	4.99	0.05	8.69	0.20	4.26
35°–25°S	0.08	5.92	0.32	5.15	0.08	11.88	0.18	4.53

of TMI data to drifter and XBT observations. The differences in the Northern Hemisphere are largest during early summer when the solar insolation usually leads to smallest mixed layer depths and largest near-surface stratification. The seasonal cycle in the differences therefore does not necessarily point toward errors in the TMI data, but, in principle, could be of a physical nature. However, as explained in detail by Gentemann et al. (2002, unpublished manuscript), it is especially the effect of surface roughness that is difficult to detect and therefore to calibrate.

4. Summary

It has long been recognized that microwave measurements play a very important role for studies of the ocean and climate since they are mostly all-weather observations of the ocean that are not significantly effected by atmospheric constituents. The microwave technology especially offers a solution to the usual cloud and aerosol problem affecting infrared retrievals of ocean SST. But although the first such instrument was flown already on *Seasat* in 1978, that is, more than 25 years ago, it is only since the launch of the TRMM mission that the application of microwave technology became possible for quantitative measurements of SST. In that sense it is a new technology. Yet, as demonstrated in this paper we find a smaller rms error relative to in situ data than can be found using RS94 fields.

The largest benefit of the microwave technology clearly comes from the unprecedented near all-weather sampling of ocean phenomena that yields measurements of the oceans' SST without the heavy smoothing in space and time that has traditionally resulted in fields that resolve only features on spatial scales larger than approximately 500 km. This is demonstrated in Fig. 7 revealing important fast and small-scale SST phenomena in the TMI fields that are absent in the smooth RS94 analyses.

Our comparison of the new TMI fields with the RS94 analysis results in a mean offset of 0.18°C and a STD difference of 0.54°C. However, regionally we find STD differences between both SST fields that reach 1°C or more, a number that is significantly larger than the error specification of either dataset alone. The RS94 analyses of SST are being considered to be accurate to $\pm 0.5^\circ\text{C}$

(Vazquez-Cuervo and Sumagaysay 2001; Reynolds et al. 2002), which is close to our findings from the comparisons with in situ surface temperature data results in STD differences between RS94 and in situ data of 0.55°C. This has to be compared to only 0.45°C from TMI fields (i.e., 30%–50% in error variance). Interpreting the differences between SST and in situ data shown in this paper, it should also be recalled that the in situ point measurements are affected by small-scale variability that is not included in the SST fields. Some fraction of the differences therefore inevitably represent “errors” in the in situ data rather than just problems in SST fields due to eddies and vertical stratification.

Until recently, the advantage of microwave SST observations was limited to latitudes lower than 38°. However, with the launch of the Earth Observing System (EOS) *Aqua* platform, the Advanced Microwave Scanning Radiometer for EOS (AMSR-E) is now in orbit, which extends the advantage of TMI data into high latitudes. AMSR-E is a passive, conical scanning, 12-channel microwave radiometer that will allow the monitoring of climate-relevant SST anomalies in high latitudes in a way unavailable before due to near-permanent cloud cover there. This will open new studies of SST variability due to deep convection, for example, in the Labrador Sea, or other high-latitude variations in SST associated with atmospheric forcing variability. For the first time we are capable of observing the high-latitude ocean with temporal resolution sufficient to capture small time- and space scales over the global ocean and especially to study climate-relevant regions that are normally covered by clouds.

The Reynolds dataset has proved to be extremely valuable for climate research. However, TMI results clearly indicate the improvements that can be possible in the future with a blended infrared–microwave (IR–MW) SST dataset. The difficulties in combining the MW and IR dataset into a new generation multisensor data fusion product are being addressed by the Global Ocean Data Assimilation Experiment (GODAE) Science team (GODAE 2001). This international group is working together on the GODAE High-Resolution SST Pilot Project (GRHSST-PP), a demonstration system for generating merged and analyzed in situ, IR, and MW SST fields at 10-km spatial and 12-h temporal resolution (Donlon 2002).

Acknowledgments. D. S. acknowledges the hospitality of the College of Oceanic and Atmospheric Sciences at the Oregon State University, where this work was initiated during a research visit. Stimulating discussions with M. Schlax and D. Chelton, who also provided the gridded weakly TMI fields, are gratefully acknowledged. The authors are also grateful to P. Niiler and R. Davis who generously provided in situ data from surface drifter and PALACE floats. D. Behringer provided the NCEP version of XBT/TAO fields. Valuable comments from R. Reynolds and an anonymous referee are gratefully acknowledged. Supported in part by Grant NAG5-8901 from the National Aeronautics and Space Administration, and a contract with the Jet Propulsion Laboratory (1205624).

REFERENCES

- Chelton, D., F. J. Wentz, C. Gentemann, R. de Szoeke, and M. Schlax, 2000: Satellite microwave SST observations of trans-equatorial tropical instability waves. *Geophys. Res. Lett.*, **27**, 1239–1242.
- Davis, R. E., J. T. Sherman, and J. Dufour, 2001: Profiling ALACEs and other advances in autonomous subsurface floats. *J. Atmos. Oceanic Technol.*, **18**, 982–993.
- Donlon, C., 2002: The GODAE High Resolution Sea Surface Temperature Pilot Project (GHRSSST-PP). *Proc. GODAE Symp.*, Biarritz, France, GODAE.
- GODAE, 2001: GODAE high resolution SST workshop. GODAE Rep. 7, GODAE International Project Office, Bureau of Meteorology, Melbourne, Australia, 65 pp.
- Kummerow, C., W. Barnes, T. Kozu, J. Shiue, and J. Simpson, 1998: The Tropical Rainfall Measuring Mission (TRMM) sensor package. *J. Atmos. Oceanic Technol.*, **15**, 808–816.
- McPhaden, M. J., and Coauthors, 1998: The tropical ocean global atmosphere observing system: A decade of progress. *J. Geophys. Res.*, **103**, 14 169–14 240.
- Murtugudde, R., J. P. McCreary, and A. J. Busalacchi, 2000: Oceanic processes associated with anomalous events in the Indian Ocean with relevance to 1997–1998. *J. Geophys. Res.*, **105**, 3295–3306.
- Niiler, P. P., 2001: The world ocean surface circulation. *Ocean Circulation and Climate*, J. Church, G. Siedler, and J. Church, Eds., Academic Press, 193–204.
- Reynolds, R. W., and T. M. Smith, 1994: Improved global sea surface temperature analysis using optimum interpolation. *J. Climate*, **7**, 929–948.
- , N. A. Rayner, T. M. Smith, D. C. Stokes, and W. Wang, 2002: An improved in situ and satellite SST analysis for climate. *J. Climate*, **15**, 1609–1625.
- Saji, N. H., B. N. Goswami, P. N. Vinayachandra, and T. Yamagata, 1999: A dipole mode in the tropical Indian Ocean. *Nature*, **401**, 360–363.
- Schlax, M. G., and D. B. Chelton 1992: Frequency domain diagnostics for linear smoothers. *J. Amer. Stat. Assoc.*, **87**, 1070–1081.
- Schott, A. F., and J. P. McCreary Jr., 2001: The monsoon circulation of the Indian Ocean. *Progress in Oceanography*, Vol. 51, Pergamon Press, 1–123.
- Vazquez-Cuervo, J., and R. Sumagaysay, 2001: A comparison between sea surface temperatures as derived from the European Remote Sensing Along-Track Scanning Radiometer and the NOAA/NASA AVHRR oceans patherfinder dataset. *Bull. Amer. Meteor. Soc.*, **82**, 925–944.
- Webster, P. J., A. M. Moore, J. P. Loschnigg, and R. R. Leben, 1999: Coupled ocean–atmosphere dynamics in the Indian Ocean during 1997–1998. *Nature*, **6751**, 356–360.
- Wentz, F. J., 1998: Algorithm theoretical basis document: AMSR ocean algorithm. Remote Sensing Systems Tech. Rep. 110398, Santa Rosa, CA, 28 pp.
- , C. Gentemann, D. Smith, and D. Chelton, 2000: Satellite Measurements of sea surface temperature through clouds. *Science*, **288**, 847–850.
- , P. D. Ashcroft, and C. L. Gentemann, 2001: Post-launch calibration of the TMI Microwave Radiometer. *IEEE Trans. Geosci. Remote Sens.*, **39**, 415–422.